XANES study on Ruddlesden-Popper phase, $La_{n+1}Ni_nO_{3n+1}$ (n = 1, 2 and ∞)

Jung-Chul Park,[a*] Dong-Kuk Kim,[b] Song-Ho Byeon[c] and Don Kim[d]

[a]Department of Chemistry of New Materials, College of Natural Sciences, Silla University, Pusan 617-736, Korea, [b]Department of Chemistry, College of natural Sciences, Kyungpook National University, Taegu 702-701, Korea, [c]College of Environment and Applied Chemistry, Kyung Hee University, Kyung Ki 449-701, Korea, [d]Department of Chemistry, Pukyong National University, Pusan 608-737, Korea. Email:jcpark@silla.ac.kr

Ruddlesden-Popper phase, $La_{n+1}Ni_nO_{3n+1}$ (n=1, 2, and ∞) compounds were prepared by citrate sol-gel method. We revealed the origin of the variation of the electrical conductivities in $La_{n+1}Ni_nO_{3n+1}$ (n=1, 2, and ∞) using resistivity measurements, Rietveld analysis, and X-ray absorption spectroscopy. According to the XANES spectra, it is found that the degree of $4p_\pi$ - $4p_\sigma$ energy splitting between 8345 eV and 8350 eV is qualitatively proportional to the elongation of the out-of-plane Ni-O bond length. With the decrease of $4p_\pi$ - $4p_\sigma$ splitting, the strong hybridization of the σ-bonding between Ni-3d and O-2p orbitals creates narrow antibonding σ* bands, which finally results in the lower electrical resistivity.

Keywords: Ruddlesden-Popper phase, $La_{n+1}Ni_nO_{3n+1}$ (n=1, 2, and ∞), XANES

1. Introduction

Lanthanum nickelates with the general formula, $La_{n+1}Ni_nO_{3n+1}$ (n=1, 2, and ∞) belong to the Ruddlesden-Popper phase, which are made up of n conducting perovskite like layers ($LaNiO_3$) separated by insulating rock-salt like layers (LaO) along the crystallographic *c*-axis.

The electrical conductivities of $La_{n+1}Ni_nO_{3n+1}$ (n=1, 2, and ∞) are mainly dependent upon the valence of the nickel ion, the number of the $LaNiO_3$ layers (n), and the oxygen content.

$LaNiO_3$, which corresponds to the n=∞ member, exhibits a rhombohedrically distorted perovskite structure, and the electrical behaviors in some derived systems are of great current interest. For instance, some systems derived from $LaNiO_3$, such as $RNiO_3$ (R=rare earth) (Lacorre et al., 1991; Torrance et al., 1992), $LaNi_{1-x}M_xO_3$ (M=Cr, Mn, Fe, Co, Cu, and Sb), (Zhang & Greenblatt, 1994; Rao et al., 1975), and $R_{1-x}M_xNiO_3$ (R = rare earth, M = Sr, Th) (Alonso et al., 1975), have been extensively studied. The electrical and magnetic properties in these systems may be closely related to the structure-driven M-I transitions and to the ratio of Ni^{2+}/Ni^{3+}.

La_2NiO_4 (n=1) crystallizes in the tetragonal K_2NiF_4 structure, which consists of alternate LaO rock-salt and $LaNiO_3$ perovskite layers along the *c*-axis. Structural, electrical, and magnetic properties of K_2NiF_4-type oxides have been researched for many years and a great interest has been renewed for these studies since the recent discovery of superconductivity of the model compound, La_2CuO_4.

It is well known that for La_2CuO_4 and La_2NiO_4, their electrical and magnetic properties are very closely related to the oxygen contents which strongly depend on the preparation conditions. $La_2NiO_{4+\delta}$ exists over a wider range of oxygen content ($0\le\delta\le0.25$) compared with that of $La_2CuO_{4+\delta}$ ($0\le\delta\le0.08$). They exhibit the extraordinary electrical conductivities, that is, the semiconducting La_2CuO_4 transforms into the superconducting $La_2CuO_{4.08}$ ($T_c \cong 44$ K) (Park et al., 1991), whereas there is no superconducting transition even for electrochemically oxidized $La_2NiO_{4.25}$ (Demourgues et al., 1996)

The crystal symmetry of $La_3Ni_2O_{7-\delta}$ compound (n=2) depends on the nonstoichiometry of oxygen, δ. The crystal symmetry of $La_3Ni_2O_{7-\delta}$ ($\delta\le0.16$) is orthorhombic with space group Fmmm, and its electrical property shows a semiconducting behavior. Upon reduction of orthorhombic $La_3Ni_2O_{7-\delta}$, a structural phase transition from orthorhombic-to-tetragonal symmetry occurs. In the fully reduced phase, $La_3Ni_2O_{6.35}$ with a semiconducting behavior, the loss of the apical oxygens leads to tetragonal with space group I4/mmm (Zhang et al., 1994). It should be pointed out that in lanthanum nickelate R.P phases, $La_{n+1}Ni_nO_{3n+1}$ (n=1, 2, and ∞), the electrical conductivities are qualitatively altered with increasing the stacking number of perovskite layer (n) along the c direction. As a consequence, the electrical conductivity is modified, such as a semiconductor (La_2NiO_4), a semiconductor, ($La_3Ni_2O_{6.9}$, n=2 with higher conductivity than La_2NiO_4), and metallic ($LaNiO_3$, n=∞).

In this work, we discuss Ni K-edge XANES spectra of $La_{n+1}Ni_nO_{3n+1}$ (n=1, 2, and ∞) in order to examine the variation of the electronic structure using the electrical resistivity measurements and Rietveld analysis as complementary tools.

2. Experimental

Single-phases $La_{n+1}Ni_nO_{3n+1}$ (n=1, 2, and ∞) were prepared by citrate based sol-gel process. Stoichiometric amounts of La_2O_3 and NiO were dissolved in nitric acid and the citric acid was added in the solution (~300%). The pH of this solution was adjusted to 4-5 by the addition of NH_4OH. After complete drying of solution at mild condition and pyrolysis, the heat treatment was performed at 650 °C for 18 hr. For $LaNiO_3$, the resulting powder was pressed into pellets and heated at 950 °C for 48 hr in air with intermittent grinding. For La_2NiO_4, the resulting powder was pressed into pellets and heated at 1050 °C for 48 hr in air. For $La_3Ni_2O_7$, the resulting product was pressed into pellets and heated at 1150 °C for 5 days with intermittent grinding.

The formation of a single phase was confirmed by powder X-ray diffraction (XRD). The patterns for structure refinement were recorded on a rotating anode installed diffractometer with an X-ray source of 40 kV, 300 mA. The Cu Kα radiation used was monochromated by a curved-crystal graphite. The data were collected with a step-scan procedure in the range $2\theta = 20 \sim 100$ ° with a step width of 0.02° and a step time of 1 s. The refinement of reflection positions and intensities were carried out using the Rietveld analysis program RIETAN (Izumi et al., 1987). The oxygen contents of samples were determined by iodometric titration. The electrical resistivities of samples were measured by four probes dc-method using a nanovoltmeter (Keithley 182) and a current source (Keithley 224).

X-ray absorption near edge structure (XANES) spectra of Ni K-edge were measured at Beam Line 7C of the Photon Factory in Tsukuba, Japan operated at 2.5 GeV, 260~370 mA. Samples were ground to fine powders in a mortar with nujol as a diluent, and then spread uniformly onto an adhesive tape, which was folded into some layers to obtain an optimum absorption jump ($\Delta\mu t \approx 1$).

Table 1
Crystallographic data and Ni-O bond lengths of $La_{n+1}Ni_nO_{3n+1}$ (n=1, 2, and ∞)

	$LaNiO_{3.00}$	$La_3Ni_2O_{6.94}$	$La_2NiO_{4.15}$
Space group	$R\bar{3}C$	Fmmm	Fmmm
a (Å)	5.4534(4)	5.3934(6)	5.45940(9)
b (Å)		5.4364(6)	5.46505(9)
c (Å)	13.1369(7)	20.516(2)	12.6870(2)
Ni-O bond length (Å)	Ni-O(x6)=1.932(2)	Ni-O(1)=2.001(6) Ni-O(3)(x4)=1.9167(4) Ni-O(2)=2.080(9)	Ni-O(1)(x2)=2.187(7) Ni-O(2)(x4)=1.9312(1)

Table 2
Atomic positions, isotropic temperature factors, and reliability factors of $La_{n+1}Ni_nO_{3n+1}$ (n=1, 2, and ∞)

compounds (*R* factors)	atom	*x*	*y*	*z*	*B*(Å^2)
$LaNiO_{3.00}$	La	0.0	0.0	0.25	0.50(2)
R_P = 9.90 %	Ni	0.0	0.0	0.0	0.56(4)
R_I = 2.69 %	O	0.453(9)	0.0	0.25	0.96(9)
R_E = 6.87 %					
$La_3Ni_2O_{6.94}$	La1	0.0	0.0	0.5	0.24(8)
R_P = 11.44 %	La2	0.0	0.0	0.3191(1)	0.52(6)
R_I = 7.40 %	Ni	0.0	0.0	0.0975(3)	0.8(1)
R_E = 6.06 %	O1	0.0	0.0	0.0	1.4(8)
	O2	0.0	0.0	0.199(1)	2.5(1)
	O3	-0.25	0.25	0.0995(8)	1.3(4)
$La_2NiO_{4.15}$	La	0.0	0.0	0.36078(6)	0.40(2)
R_P = 6.90 %	Ni	0.0	0.0	0.0	0.44(5)
R_I = 2.82 %	O1	0.0	0.0	0.1724(5)	2.40(9)
R_E = 5.05 %	O2	0.25	0.25	0.0	0.68(9)

All data were recorded with a spacing of ~0.4 eV in a transmission mode at room temperature, using a Si (311) channel-cut monochromator. A Ni foil was used to calibrate the photon energy for each measurement.

3. Results and discussion

The crystallographic data and Ni-O bond lengths are given in Table 1. The refined atomic coordinates, isotropic temperature factors, and final reliability factors are listed in Table 2. Corrections for (00*l*) preferred orientation were made for $La_3Ni_2O_{6.94}$ and $La_2NiO_{4.15}$ in the final stage of the refinement.
X-ray diffraction data of three samples were analysed by means of the Rietveld method and they show different symmetries depending on the stacking number of perovskite layers (n). The observed symmetry is rhombohedral ($R\bar{3}C$) for $LaNiO_3$. On the contrary, the orthorhombic symmetry (Fmmm) was observed in $La_3Ni_2O_{6.94}$ and $La_2NiO_{4.15}$ phase. As shown in Table 1, Ni-O bond length in $LaNiO_3$ is about 1.932 Å as the Ni^{3+} ions are in near-octahedral coordination. With increasing the stacking number of perovskite layers (n) and introducing rock-salt layers, regular "NiO_6" octahedrons are distorted, which results in the slight variation of Ni-bond lengths in $La_3Ni_2O_{6.94}$ and $La_2NiO_{4.15}$ phase compared with that of $LaNiO_3$. This structural variation may give rise to the modification of the electronic structure which is greatly related to the electrical resistivity.

The temperature dependences of the electrical resistivity of $La_{n+1}Ni_nO_{3n+1}$ (n=1, 2, and ∞) are shown in Fig. 1. $LaNiO_3$ with a Ni valence of +3 (nearly 100%), is metallic down to 10 K. $La_3Ni_2O_{6.94}$ ($Ni^{3+} \cong 44\%$) is metallic with a nearly temperature-independent resistivity that is higher by a factor of 100 relative to the values of $LaNiO_3$ at room temperature. $La_2NiO_{4.15}$ ($Ni^{3+} \cong 30$ %) shows semiconducting behavior.
In comparison with 3-phases, the fully reduced $La_3Ni_2O_{6.3}$ phase was prepared from $La_3Ni_2O_{6.94}$ under 10 % H_2/N_2 atmosphere at

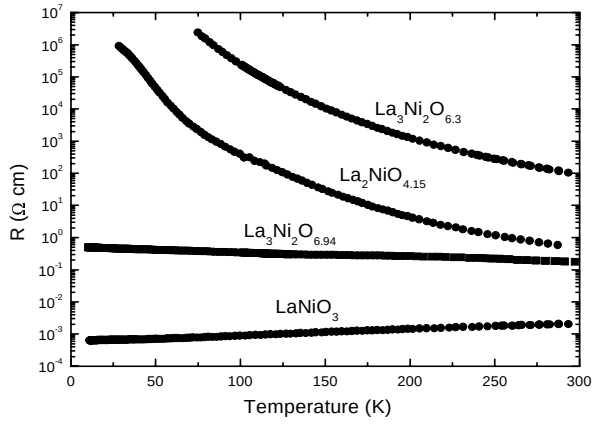

Figure 1
Electrical resistivity as a function of temperature.

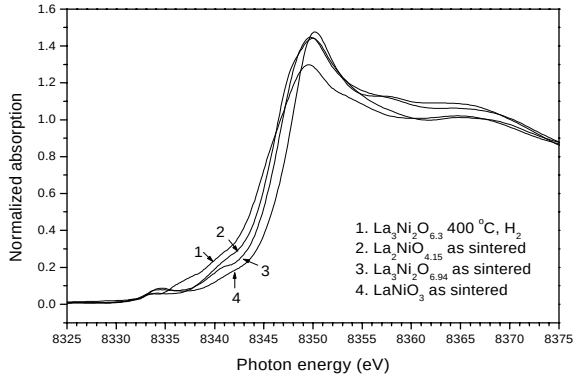

Figure 2
Ni K-edge XANES spectra for $La_3Ni_2O_{6.3}$ (1), $La_2NiO_{4.15}$ (2), $La_3Ni_2O_{6.94}$ (3), $LaNiO_3$ (4)

400 °C and we measured its electrical resistivity, which exhibits semiconducting behavior with the highest resistivity at room temperature. The electrical resistivity measurements indicate that the transport properties depend on the stacking number of perovskite layer (n) as well as the concentration of Ni^{3+}.

In order to examine the modification of the electronic structure of $La_{n+1}Ni_nO_{3n+1}$ (n=1, 2, and ∞), Ni K-edge XANES has been used. Fig. 2 shows Ni K-edge spectra for $La_{n+1}Ni_nO_{3n+1}$ (n=1, 2, and ∞). From the Ni K-edge XANES spectra, it is shown that the overall spectral feature shifts to higher energies upon increasing the concentration of Ni^{3+} as well as the stacking number of perovskite layer (n). The second derivatives in Fig. 3 show that the pre-edge peak at ~8335 eV, which is assigned to 1s → 3d quadrupole transition, shifts to higher energies and also increases in area with increasing the stacking number n as well as the concentration of Ni^{3+}, indicating the increased density of Ni 3d states. In addition, the main absorption peak between 8345 eV and 8350 eV actually consists of two peaks except for the case of $LaNiO_3$. For the detailed assignment of the two peaks, the polarized Ni K-edge spectra were measured for a single crystal, La_2NiO_4 as shown in Fig. 4, where spectra between $\phi = 10^o$ and $\phi = 90^o$ approximately correspond to those for X-ray polarization vector ε parallel to the c axis (ε∥c) and to the ab plane (ε⊥c),

respectively. Based on both dipole selection rule and symmetry consideration, 1s $\rightarrow 4p_\pi$ transition is allowed for $\varepsilon \| c$ and 1s$\rightarrow 4p_\sigma$ one for $\varepsilon \perp c$, which is in agreement with assignments as previously reported (Sahiner et al., 1995). The reason why the main peak consists of two peaks can be explained by energy separation between out-of-plane Ni $4p_\pi$ and in-plane Ni $4p_\sigma$ states. As the concentration of Ni^{3+} increases, in-plane and out-of-plane Ni-O bond lengths become closer so that $4p_\pi$ - $4p_\sigma$ energy splitting is gradually vanished, which is in agreement with Ni-O bond lengths determined by Rietveld analysis. The degree of the $4p_\pi$ - $4p_\sigma$ energy splitting in these materials may be qualitatively proportional to the elongation of out-of-plane Ni-O bond length.

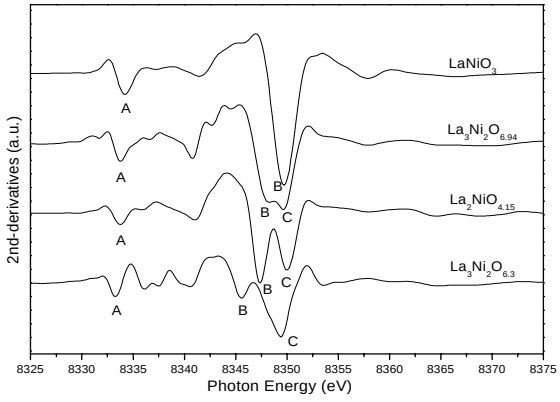

Fig 3
The second-derivatives of Ni K-edge XANES spectra for samples.

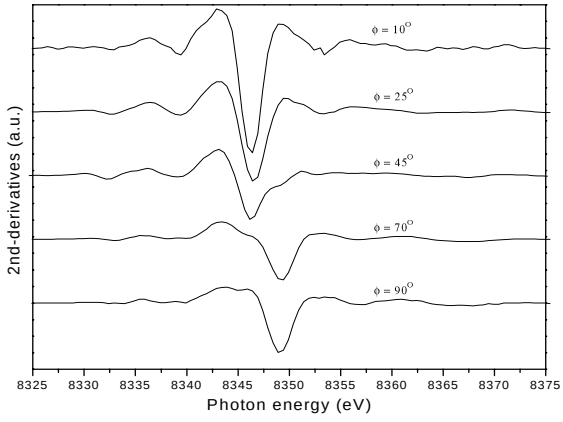

Fig 4
The second derivatives of polarized Ni K-edge spectra for a single crystal La_2NiO_4. The value of ϕ indicates the angle between incident beam and *ab* plane of single crystal.

This means that with the decrease of $4p_\pi$ - $4p_\sigma$ splitting as shown in the second derivatives (Fig. 3), the strong hybridization of the σ-bonding between Ni-3d and O-2p orbitals creates narrow antibonding σ^* bands (Zhang et al., 1994), which finally results in the lower electrical resistivity.

4. Conclusions

According to the XANES spectra, the energy of the pre-edge region which corresponds to the 1s $\rightarrow$ 3d transition around 8335 eV, shifts to the higher one depending on the stacking number (n) as well as the concentration of Ni^{3+}. As shown in the second-derivatives in Ni K-edge absorption region between 8345 eV and 8350 eV, the main peak actually consists of two peaks except for $LaNiO_3$. Two peaks can be assigned to 1s $\rightarrow 4p_\pi$ transition and 1s $\rightarrow 4p_\sigma$ one, respectively. Thus, with increasing the concentration of Ni^{3+}, in-plane and out-of-plane Ni-O bond lengths become closer, and $4p_\pi$ - $4p_\sigma$ energy splitting is gradually decreased, which consequently results in the decrease of the electrical resistivity.

This work was supported by grant No. 971-0305-026-2 from the Basic Research program of the KOSEF.

References

Alonso, J.A., Martinez-Lope, M.J., Hidalgo, M. (1995). *J. Solid State Chem.* 116, 146
Demourgues, A., Dordor, P., Doumerc, J.P., Gremier, J.C., Marquestaut, E., Pouchard, M., Villesuzanne, A., Wattiaux, A. (1996). *J. Solid State Chem.* 124, 199.
Izumi, F., Murata, H., Watanabe, N. (1987). *J. Appl. Crystallogr*. 20, 411.
Lacorre, P., Torrance, J.B., Rannetier, J., Nazzal, A.I., Wang, P.W., Huang, T.C. (1991). *J. Solid State Chem.* 91, 225
Park, J.C., Hwong, P.V., Ray-Lafon, M., Grenier, J.C., Watiaux, A., Pouchard, M. (1991). *Physica C*, 177, 487.
Rao, C.N.R., Rarkash, OM., Ganguly, P. (1975). *J. Solid State Chem.* 116, 146
Sahiner, A., Croft, M., Guha, S., Perez, I., Zhang, Z., Greenblatt, M., Metcalf, P.A., Jahns, H., Liang, G. (1995). *Phys. Rev. B51*, 5879
Torrance, J.B., Lacorre, P., Nazzal, A.I., Ansaldo, E.J., Niedermayer, Ch. (1992), *Phys. Rev.* B45, 14.
Zhang, Z., Greenblatt, m., Goodenough, J.B. (1994). J. Solid State Chem. 108, 402.
Zhang, Z., Greenblatt, M. (1994). J. Solid State Chem. 111, 145.

 Received 31 July 2000 • Accepted 30 October 2000